20th IMEKO TC10 Conference
"Measurement for Diagnostics, Optimization and Control to Support Competitiveness and Innovation"
Lisbon, Portugal, September 28–29, 2026

Anomaly detection of ventilation fan by training a variational auto-encoder with current waveforms of brushless DC motor

Yukio Hiranaka[1,2], Koichi Tsujino[2]

Ojiro Miyazaki[3], Tadashi Yasufuku[3], Fumiaki Tsukazaki[3], Kazuyuki Kouno[3]

[1]Hiranaka Technology Research, Susono, Japan
[2]AiSpirits, Tokyo, Japan
[3]Nuvoton Technology Corporation Japan, Kyoto, Japan

***Abstract* – Anomalies in motor-driven equipment can be detected potentially by measuring the current of the driving motor. We attempt to utilize unsupervised learning of motor current to detect load fluctuations and bearing anomalies in ventilation fans. By training a variational auto-encoder on the cyclic current waveforms of a motor under normal conditions, anomalies—such as deviations in cycle length, peak current, and waveform patterns—can be detected using anomaly scores derived from latent variables. This approach is applied to experimental data from a small brushless DC motor used in a ventilation fan to verify its effectiveness.**
Keywords – Anomaly Score, Motor Current, Ventilation Fan, Variational Auto-Encoder, Industry Innovation and Infrastructure.

I. INTRODUCTION

Detecting anomalies in equipment is crucial for condition-based maintenance and is expected to have applications in various fields. In particular, motor-driven equipment often operates for a long period of time, and any failure may force the equipment to shut down. Therefore, detecting equipment anomalies at an early stage is desirable. This study presents an anomaly detection method for ventilation fans driven by brushless DC motors by monitoring current waveforms using a variational auto-encoder (VAE) [1]. Specific methods and illustrating results are presented.

II. RELATED STUDIES

Various methods exist for detecting anomalies in rotating machinery, and most of them focus on spectral analysis of vibrations [2,3]. However, vibration analysis is complicated by numerous factors, such as resonance and harmonics. A more reliable approach with a clearer causal relationship is the analysis of the motor's current waveform. Selecting specific waveform features is critical for accurate diagnostics. Prior studies have demonstrated this through various approaches, including motor fault detection via spectral analysis [4,5], bearing defect detection using statistical parameters (e.g., root mean square, crest factor, kurtosis, and skewness) [6], and eccentricity detection based on wavelet-derived features combined with cluster classification [7].

Also, when input information is multidimensional, it is necessary to extract appropriate information that represents the anomalous state, and the choice of information compression method greatly affects the results. While effective features were traditionally selected through human analysis, recent AI-based methods have enabled efficient extraction of comprehensive information directly from the data. Since anomalies can manifest in various unpredictable forms, their specific characteristics cannot be predefined. Therefore, an unsupervised learning method is required to establish a baseline using only available normal data. Among various AI techniques, VAEs are particularly promising for their ability to extract essential latent variables from the distribution of normal data [6]. In the proposed method, raw current waveforms are used directly as inputs to the AI, bypassing the need for manual feature selection. This approach enables the model to automatically learn and extract the most suitable features for quantifying anomalies.

III. DESCRIPTION OF THE METHOD

A. Raw motor current

When measuring the current flowing through the power line of a single-phase brushless DC fan (SanAce80 9GA0812P6G001, 80x80x20mm, PWM speed controllable), the current is observed to switch ON/OFF according to the PWM signal as shown in Fig. 1.

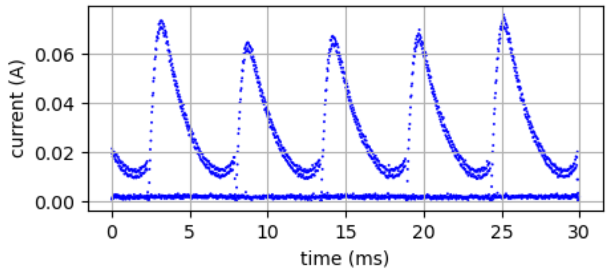

Fig. 1. Example of the motor current at 40% PWM duty ratio.

Since the current changes depending on the observation timing, a clear set of cyclic waveforms can be obtained by taking only the maximum current from each PWM cycle as the representative value (Fig. 2).

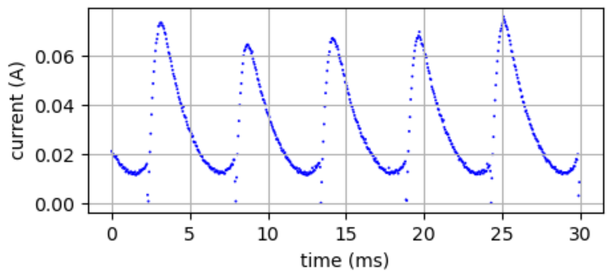

Fig. 2. Trace of maximum current value of each PWM cycle.

B. Maximum current cycle waveform

The motor consists of four outer rotor poles, resulting in four current cycles per revolution. These cycles exhibit the fluctuations in peak current values observed in Fig. 2. For precise anomaly detection, it is necessary to determine which cycle waveform to use for anomaly detection. To isolate the current waveform for each rotor pole, the second-order difference of the data in Fig. 2 is calculated. The resulting local maxima are defined as the endpoints of each cycle, as indicated by the orange crosses in Fig. 3.

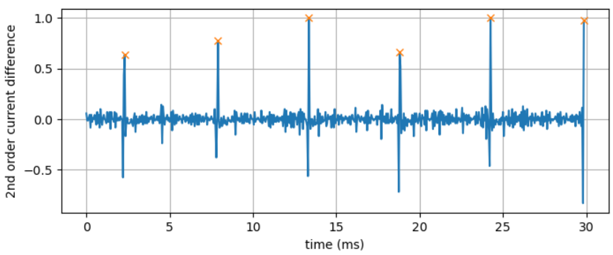

Fig. 3. Second order difference of Fig.2.

From the current waveform of at least four consecutive cycles, the cycle in which the peak current value is higher than the others is extracted and taken out as the maximum current cycle waveform (Fig. 4).

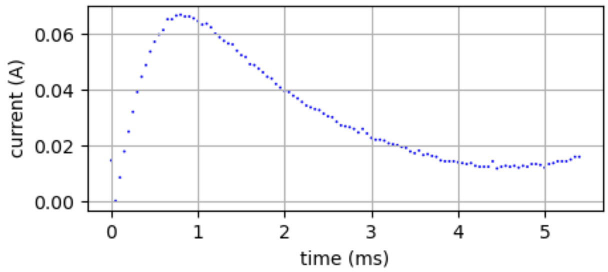

Fig. 4. Example of the maximum current cycle.

C. Rise time alignment

The start of the current cycle depends on the rotational state and does not coincide with the current sampling timing. Therefore, the starting point of the obtained current cycle fluctuates by about one PWM cycle. To eliminate this fluctuation, sampling time correction was performed by linear interpolation of the current data, as shown in Fig. 5.

Specifically, the starting point of each cycle is synchronized to a predefined current level (START_LVL = 0.05 A), with its precise location calculated using an internal division ratio (a:b) between sampling points. The interpolated current values (red circles) for each PWM period are aligned with the starting value and used as training and test data for anomaly score calculation.

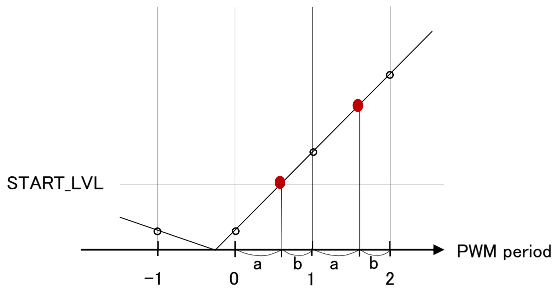

Fig. 5. Rise time alignment by linear interpolation.

D. VAE anomaly score

Similar to the anomaly detection using vibrational frequency spectra [8], a VAE is trained to form the latent spatial distribution of the training data to follow a standard normal distribution. The anomaly score can be calculated as the normalized Euclidean distance from the center of the normal distribution.

Specifically, as shown in equation (1), the deviation of the latent value z_i on i axis of the VAE latent space

(D dimensions) from the mean $\overline{z_i}$ is corrected by the variance σ_i, which corresponds to the normalized distance from the distribution center and is taken as the anomaly score V_D. However, when the number of dimensions is redundant, this score is overestimated. This overestimation is mitigated by D_{cmps}, the redundancy metric calculated via Equations (2) and (3).

$$V_D = \sqrt{\frac{1}{D_{cmps}} \sum_{i=1}^{D} \left(\frac{z_i - \overline{z_i}}{\sigma_i}\right)^2}, \qquad (1)$$

$$D_{cmps} = \frac{1}{D} \sum_{i=1}^{D} \sum_{j=1}^{D} R^2(f_i, f_j), \qquad (2)$$

$$R(f_i, f_j) = \frac{1}{N} \sum_{n=1}^{N} f_i(n)\, f_j(n), \qquad (3)$$

where $f_i(n)$ is the input basis function which corresponds to the i-th latent variable = 1, N is the number of input variables, and $R(f_i, f_j)$ represents the correlation of two basis functions.

Fig. 6 shows the structure and training flow of the VAE, where the encoder compresses the input variables to latent variables of D dimensions.

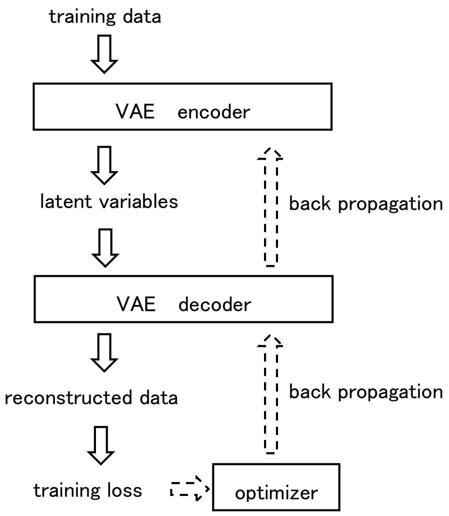

Fig. 6. Processing flow of the VAE.

As shown in Fig. 4, the current cycle waveform had over 100 points, so the input variable was set to 100. The VAE was configured with a 3-layer structure containing 16 units in the hidden layer, utilizing a linear activation function. Network training was performed using the Adam optimizer with a mini-batch size of 1 over 10,000 iterations.

The latent space dimensionality D was set to three, because certain anomalies that were inseparable in a two-dimensional space became distinguishable when projected into three dimensions. Depending on the situation of the subject, differences can be observed in the peak value, peak time, and tail value of the current waveform at least, so the selection of three dimensions is considered suitable.

IV. EXPERIMENTS AND DISCUSSIONS

Fig. 7 illustrates the experimental setup. An expansion pipe fitting (made of polyvinyl chloride, expanding the inner diameter from 77 mm to 90 mm) was taped to the discharge side of the fan (inner diameter: 77 mm) to serve as a flow straightener. A shield plate (made of polyethylene terephthalate, 182 mm high × 257 mm wide, 1 mm thick) was placed downstream of this fitting, and current measurements were taken while varying the position of the shield plate. Note that when the shield plate was placed directly downstream of the fan without using the flow-straightening pipe, it was not possible to consistently acquire current waveforms like those shown below potentially due to the influence of airflow around the fan.

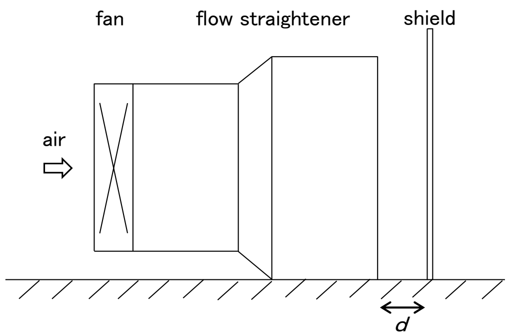

Fig. 7. Experimental setup.

Moving the shield plate closer to the outlet of the flow straightener causes the fan's airflow rate and the rotational speed to change. Generally, it is expected that the rotational speed drops and the fan current rises when the load increases while the rotational speed rises and the fan current falls when the load decreases. However, fluid dynamics often defy simple interpretation, and phenomena contrary to expectations may frequently occur.

As shown in Fig. 8, the actual current waveforms (almost completely overlapping 11 traces extracted from current data of 400 ms, except for (e) which has 10 traces) exhibit slight variations. The most notable change is observed at the 0.1A crossing point, where the timing is delayed in the order of (b), (c), and (d). This delay means the increase in cycle length (indicating a drop in rotational speed), which suggests that the load is increased.

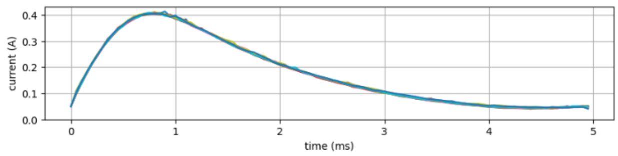

(a) without the shield

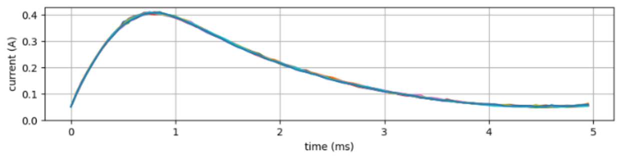

(b) with the shield at *d*=30mm

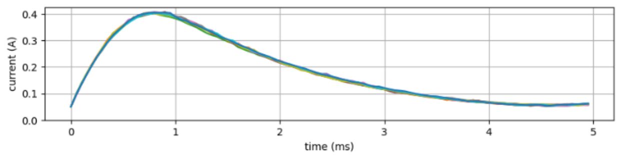

(c) with the shield at *d*=20mm

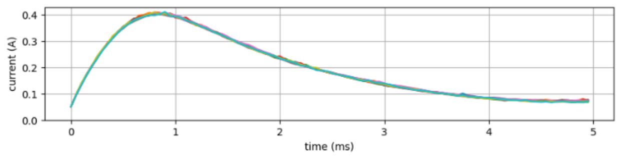

(d) with the shield at *d*=10mm

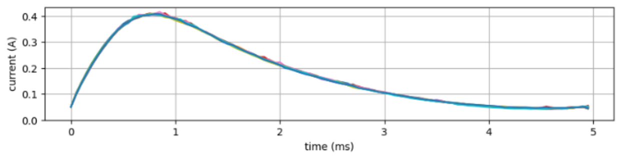

(e) with the shield at *d*=0mm

Fig. 8. Examples of (a)normal and (b,c,d,e)anomalous state currents.

Fig. 9 shows features extracted from the maximum current waveforms obtained for each shield positions (11 waveforms, or 10 for *d*=0): the current cycle period (subsequent start points are not shown in Fig. 8), the peak current value, and the minimum (bottom) current value in the tail section. While the period is measured in 5 ms increments determined by the current sampling interval, a clear trend is observed as the value of *d* decreases (*d*=3, 2, 1). When the fan's downflow is blocked (*d*=0), the period is slightly longer than when no shielding plate is placed. Although the reason for this phenomenon is unknown, it may be caused by a nonlinear or three dimensional fluid mechanism under the condition of complete blockage.

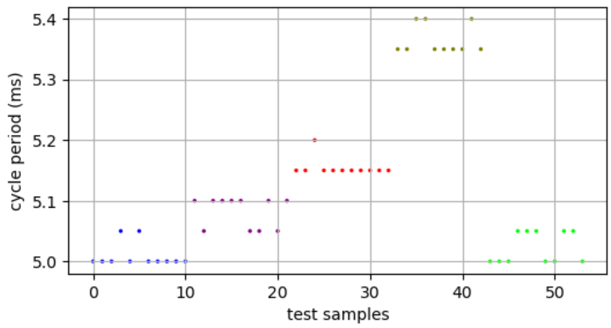

(a) cycle period

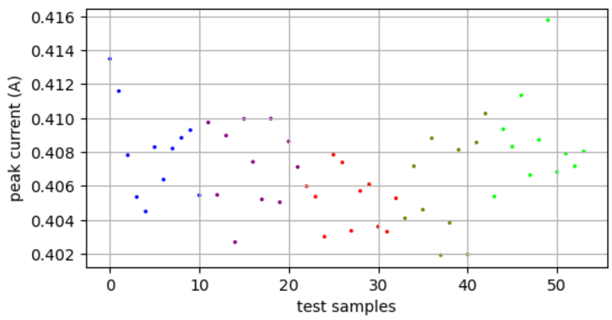

(b) peak current

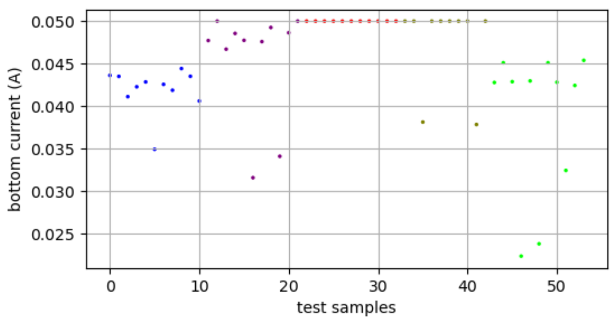

(c) bottom current

Fig. 9. Three specific features of Fig.8.

Fig. 10 shows the latent space distribution (presented via three-view projections due to its three-dimensional nature) obtained by inputting the entire dataset from Fig. 8 into the VAE encoder after training the VAE using the data from Figure 8(a) as the normal states. The plotted points are colored blue, purple, red, gray, and green, corresponding to Figures 8(a), (b), (c), (d), and (e), respectively. It is considered that the data proximity observed in Fig. 9 is reflected in this three-dimensional plot.

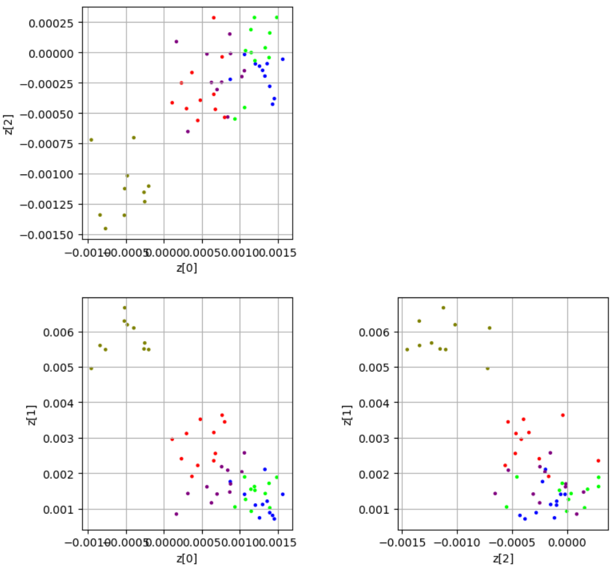

Fig. 10. Three dimentional latent space distribution.

The distance (degree of deviation) from the training data distribution can be quantified by the anomaly score (1) shown in Fig. 11. Generally, a deviation of 3 (representing three time the standard deviation) or more from the normal training data (blue) can be classified as "anomaly." While the two cases with *d*=2 and *d*=1 can clearly be identified as anomalies, the remaining two cases (*d*=3 and *d*=0) cannot be immediately classified as such, though one can observe that they deviate slightly from the normal states.

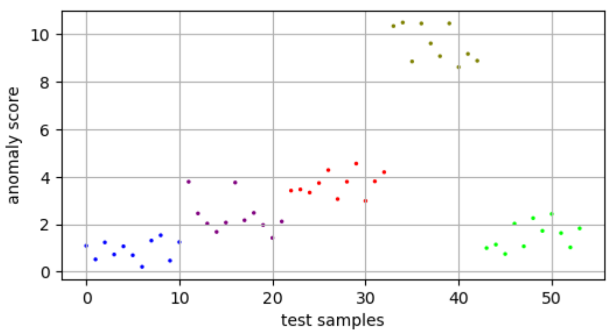

Fig. 11. Anomaly scores for normal(blue) and anomalous(green) states.

As observed in Fig. 9, the increase in the cycle period appears to be the primary factor, while the bottom current value at the tail section serves as the secondary factor for the anomaly detection. It should be emphasized here that, determining how to calculate the degree of anomaly and how to set the threshold for anomaly judgements based on these characteristics are not simple tasks.

With VAEs, it is possible to determine the optimal score for representing the degree of anomaly based on the distribution of each feature. Furthermore, the features used are not arbitrarily selected, by inputting the entire current waveform, the model extracts the optimal features, which can be regarded as an optimal weighted average because of the usage of linear activation functions in the VAE layers. Additionally, because the training data is scaled to follow a standard normal distribution, the anomaly score reflects the deviation from the normal distribution in terms of standard deviations, thereby enabling statistically proper anomaly detection.

It has been demonstrated that anomaly detection is possible even with a small amount of training data—around ten samples, while reliable anomaly detection generally requires more extensive training data. The definition of "normal" versus "anomalous" depends on the specific subject. In cases where the normal state fluctuates significantly based on the operating environment, relative anomaly detection may be preferred; this approach identifies deviations from observed normal behavior rather than relying on absolute anomaly criteria. In such environments, the ability to perform on-device learning and anomaly detection using only a minimal amount of normal training data offers practical advantages.

While this study focused on detecting current fluctuations caused by load changes, we intend to investigate the feasibility of detecting various types of anomalies, such as bearing faults, in the future.

V. CONCLUSION

This study demonstrated that anomalous fan state can be detected by measuring the motor current waveform. Specifically, the method enables robust anomaly detection by extracting peak current values for each PWM cycle, isolating individual cycles to mitigate the influence of magnetic pole configurations, correcting sampling fluctuations via linear interpolation, and finally, computing anomaly scores through a VAE.

REFERENCES

[1] **Kingma D.P.; Welling M.:** Auto-Encoding Variational Bayes, Proc. International Conference on Learning Representations, arXiv:1312.6114, 2014.

[2] **Randall, R.B.:** Vibration-based Condition Monitoring: Industrial, Aerospace and Automotive Applications, Wiley, 2ndEd, 2021.

[3] **Principi, E.; Rossetti, D.;Squartini, S.; Piazza, F.:** Unsupervised Electric Motor Fault Detection by Using Deep Autoencoders, IEEE/CAA Journal of Automatica Sinica, vol.6, no.2, pp.441-451, 2019.

[4] **Benbouzid M.E.H.; Vieira, M; Theys, C:** Induction Motors' Faults Detection and Localization Using Stator Current Advnced Signal Processing Techniques , vol.14, no.1, pp.14-20, 1999.

[5] **Benbouzid M.E.H.:** A Review of Induction Motors Signature Analysis as a Medium for Faults Detection, IEEE trans. Industrial Electronics, vol.47, no.5, pp.984-993, 2000.

[6] **Dhomad, T,A.; Jabar A.A.:** Bearing Fault Diagnosis Using Motor Current Signature Analysis and the Artificial Neural Network, International Journal on Advanced Science Engineering Information Technology, vol.10, no.1, pp.70-79, 2020.

[7] **Ebrahimi, B.M.; Roshtkhari M.J.; Faiz J.; Khatami S.V.:** Advanced Eccentricity Fault Recognition in Permanent Magnet Synchronous Motors Using Stator Current Signature Analysis, IEEE trans. Industrial Electronics, vol.61, no.4, pp.2041-2052, 2014.

[8] **Hiranaka Y.; Tsujino K.:** VAE Deviation for Detecting Bearing Anomalies, 17th IMEKO TC 10 and EUROLAB Virtual Conference, October 20-22, 2020.